Theory of the color change of Na_xWO_3 as a function of Na-charge doping

Yu Xue
Department of Physics, University at Buffalo, State University of New York, Buffalo, New York 14260, USA

Yong Zhang
National Renewable Energy Laboratory, 1617 Cole Boulevard, Golden, Colorado 80401, USA

Peihong Zhang
Department of Physics, University at Buffalo, State University of New York, Buffalo, New York 14260, USA

(Received 23 April 2009; published 21 May 2009)

We report theoretical investigations of the coloration of WO_3 upon charge insertion using sodium tungsten bronze (Na_xWO_3) as a model system. Our results explain well the systematic color change of Na_xWO_3 from dark blue to violet, red-orange, and finally to golden yellow as sodium concentration x increases from 0.3 to unity. Proper accounts for both the interband and the intraband contributions to the optical response are found to be very important for a detailed understanding of the coloration mechanism in this system.

DOI: 10.1103/PhysRevB.79.205113 PACS number(s): 78.20.Bh, 71.20.−b, 78.20.Ci, 82.47.Jk

Electrochromic materials[1,2] exhibit reversible and persistent change in the optical properties, hence their color, upon applying an electrical pulse that injects both electrons and compensating ions into the material. Potential applications of electrochromic materials range from information display and light shutters to energy-efficient smart windows.[1,2] Tungsten trioxide (Refs. 3 and 4) is one of the most extensively studied electrochromic materials due to its superior coloration efficiency, short response time, and reversibility.[1] Enhanced electrochromic properties in WO_3 nanowires have been reported recently.[5,6] Despite much research effort, a first-principles theory for the coloration mechanism in this material has not emerged. Here we report density-functional theory (DFT) (Ref. 7) investigations of the coloration mechanism of WO_3 upon charge insertion. Our results explain very well the systematic change in color[1,8,9] of Na_xWO_3 from dark blue to metallic golden yellow with increasing sodium concentration. We find that proper accounts for the free carriers' contribution to the optical response are critical for a quantitative understanding of the coloration mechanism in this system.

Undoped stoichiometric WO_3 is a transparent semiconductor. Double injection of electrons and compensating ions (e.g., H^+, Li^+, or Na^+) by an electric pulse induces a dark blue color in the electrochromic WO_3 film. Despite intense research over the last three decades, the mechanism of electrochromism remains controversial.[1,10–14] Interestingly, sodium tungsten bronze (Na_xWO_3) also shows various bluish colors at low sodium concentrations. Therefore, it is likely that both systems share the same fundamental coloration mechanism[11] and the formation of tungsten bronze might be responsible for the electrochromism in WO_3. Furthermore, the color of Na_xWO_3 changes from dark blue to violet, red-orange, and finally to golden yellow as sodium concentration x increases from 0.3 to unity.[1,8,9] A consistent theory should be able to explain the color of Na_xWO_3 for a wide range of Na concentration. Unfortunately, although the electronic and structural properties of Na_xWO_3 have been studied extensively,[8,9,15–22] a quantitative understanding of its vivid color change with varying Na content is still lacking.

Materials color from first principles. The apparent color of a material is intimately related to its optical-absorption spectra. With the advance of modern electronic-structure methods, various optical properties can be routinely calculated nowadays. However, to the best of our knowledge, there have been no reports of calculating the apparent color of materials from first principles. The complicated physiology of human color perception makes calculating the apparent color of a material rather difficult. Fortunately, the color space[23] defined by the International Commission of Illumination (CIE), the CIE 1931 XYZ color space, provides a mathematical foundation for a quantitative description of colors.

The CIE XYZ color space defines three color-matching functions, $\bar{x}(\lambda)$, $\bar{y}(\lambda)$, and $\bar{z}(\lambda)$, as shown in Fig. 1. The XYZ tristimulus values for an object illuminated by a light source with a spectral power distribution $I(\lambda)$ are then given by

$$X = \int I(\lambda)R(\lambda)\bar{x}(\lambda)d\lambda,$$

$$Y = \int I(\lambda)R(\lambda)\bar{y}(\lambda)d\lambda,$$

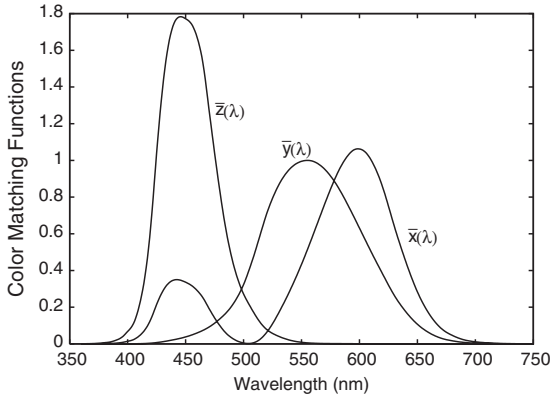

FIG. 1. The CIE XYZ color-matching functions. The CIE-defined three-color matching functions known as $\bar{x}(\lambda)$, $\bar{y}(\lambda)$, and $\bar{z}(\lambda)$. These functions can be considered as the spectral-sensitivity functions of three linear light detectors that give the CIE XYZ tristimulus values.

$$Z = \int I(\lambda)R(\lambda)\bar{z}(\lambda)d\lambda, \tag{1}$$

where $R(\lambda)$ [or $R(\omega)$] is the wavelength (frequency) dependent reflectivity of the object. The CIE XYZ color space is related to the well-known CIE RGB color space by the following linear transformation:

$$\begin{bmatrix} X \\ Y \\ Z \end{bmatrix} = \frac{1}{0.176\,97} \begin{bmatrix} 0.490\,00 & 0.310\,00 & 0.200\,00 \\ 0.176\,97 & 0.812\,40 & 0.010\,63 \\ 0.000\,00 & 0.010\,00 & 0.990\,00 \end{bmatrix} \begin{bmatrix} R \\ G \\ B \end{bmatrix}. \tag{2}$$

The reflective color and the relative brightness of a material can be constructed once we obtain the tristimulus values X, Y, and Z or, alternatively, R, G, and B.

For an ideal semi-infinite crystal, the normal-incidence reflectivity is related to the complex index of refraction $\tilde{n}$ and the macroscopic complex dielectric function $\varepsilon(\omega)=\varepsilon_1(\omega)+i\varepsilon_2(\omega)$ via

$$R(\omega) = \left| \frac{\tilde{n}(\omega)-1}{\tilde{n}(\omega)+1} \right|^2; \quad \tilde{n}(\omega) = \varepsilon^{1/2}(\omega). \tag{3}$$

The imaginary part of the dielectric function $\varepsilon_2(\omega)$ due to interband transitions can be calculated using DFT-based first-principles electronic-structure techniques

$$\varepsilon_2^{\text{inter}}(\omega) = \frac{16\pi^2}{\omega^2} \sum_{vc\vec{k}} |\vec{\lambda} \cdot \langle v\vec{k}|\vec{v}|c\vec{k}\rangle|^2 \delta[\omega - (\epsilon_{c\vec{k}} - \epsilon_{v\vec{k}})], \tag{4}$$

where $\vec{\lambda}$ is the polarization of light, $\vec{v}$ is the velocity operator, and $|c\vec{k}\rangle(|v\vec{k}\rangle)$ denotes unoccupied conduction states (occupied valence states). The real part of the dielectric function is related to the imaginary part through the Kramers-Kronig relations. In undoped semiconductors, only the interband transitions contribute to the optical response. In metals or doped semiconductors, however, the free carriers' contributions to the optical response are very important. These contributions can be conveniently modeled on the basis of the Drude theory

$$\varepsilon_2^{\text{intra}}(\omega) = \frac{\gamma\omega_p^2}{\omega(\gamma^2+\omega^2)}, \quad \omega_p^2 = 4\pi n/m^*. \tag{5}$$

In the above equations, $n=x/V_{\text{cell}}$, m^*, and $1/\gamma$ are, respectively, the density, optical effective mass, and relaxation time of the free carriers. We use the measured effective mass[15] and a relaxation broadening of $\gamma=0.3$ eV in our calculation. Combining both the interband and intraband contributions thus gives the imaginary part of the total electronic dielectric function $\epsilon_2^{\text{total}}=\epsilon_2^{\text{inter}}+\epsilon_2^{\text{intra}}$.

Electronic structure and optical properties of $Na_{1.0}WO_3$. Tungsten trioxide comprises of corner-sharing WO_6 octahedra.[1,24] Several metal ions can be incorporated into the structure to form tungsten bronzes. Among them sodium tungsten bronze (Na_xWO_3) is the most extensively studied system owing to its unusual optical properties and dramatic changes in color[1,8,9] with increasing x. Na_xWO_3 assumes a simple cubic structure for Na contents $x \geq 0.4$ and undergoes a sequence of structural changes with decreasing x.[25,26] The cubic phase can be synthesized under nonequilibrium conditions down to $x \sim 0.2$.[19,27] Our study covers Na concentration $0.3 \leq x \leq 1.0$. For simplicity, we assume a cubic structure for all Na concentrations studied. We do not expect minor structural distortions in $Na_{0.3}WO_3$ will affect the result significantly. Our calculations are based on DFT within the local-density approximation (LDA).[28] The LDA is able to reproduce qualitatively the electronic structure of Na_xWO_3 as documented by previous calculations.[21,22] We use the pseudopotential plane-wave formalism[29] as implemented in the PARATEC code.[30] Norm-conserving pseudopotentials[31,32] are used for all calculations. For the W atom, $5s$, $5p$, and $5d$ states are included in the valence states. The k-point set is generated by the Monkhorst-Pack scheme[33] with a density of $20\times20\times20$ for self-consistent-field calculation and $40\times40\times40$ for optical-transition calculations. The plane-wave energy cutoff is set at 120 Ry to ensure the convergence of the calculations. In order to avoid inconvenient (i.e., large) unit cells for systems with fractional x, we adopt the virtual-crystal approximation[34,35] in which fractional Na compositions are modeled by pseudoatoms with appropriate nuclear charges and valence electrons. We use the experimental lattice constants of Na_xWO_3 which can be conveniently expressed by the Vegard's law $a(x)=3.7845+0.0821x$.[26] The Brillouin zone summation in Eq. (4) is carried out on a dense $32\times32\times32$ uniform grid with an energy broadening of 0.3 eV.

Figure 2(a) shows the band structure of $Na_{1.0}WO_3$, the ending system of the series studied. As mentioned previously, $Na_{1.0}WO_3$ displays a distinct golden yellow color. The electronic band structure suggests, however, that the strong interband transitions mainly occur across an energy window of $4 \sim 7$ eV. This falls well above the visible energy window and cannot explain its golden yellow appearance. There are also intersubband transitions as indicated by circles in Fig. 2(a). However, the energies of these transitions are very low (less than 1.0 eV) and cannot be responsible for the optical response in the visible range either. Therefore, a proper account for the free carriers' (intraband) contributions is critical for a quantitative understanding of the optical properties of this system. Figure 2(b) shows the calculated reflectivity spectra $R(\omega)$ of $Na_{1.0}WO_3$ with and without including the free carriers' response.

It is clear that the reflectivity in the visible range (1.5 $\sim$3.0 eV) is dominated by the free carriers' contribution (which is renormalized by the interband transitions as explained below). The spectra are fairly uniform and featureless for photon energy $1.5 \leq E \leq 3.0$ eV if the free carriers' plasma response is not included. As a result, $Na_{1.0}WO_3$ would appear dark gray [more precisely, slightly bluish dark gray as shown in the inset of Fig. 2(b)] without taking into account the free carriers' contributions. These contributions significantly enhance the reflectivity below 2.5 eV and suppress the reflectivity around 3.0 eV, resulting in the golden yellow appearance of $Na_{1.0}WO_3$ as shown in the inset of Fig. 2(b). The onset of the free carriers' enhanced reflectivity corresponds to the renormalized (screened) plasma frequency $\tilde{\omega}_p$, defined by $\text{Re}[\epsilon^{-1}(\tilde{\omega}_p)]=0$. The renormalized plasma frequency is related to the bare value [defined in Eq. (5)] by

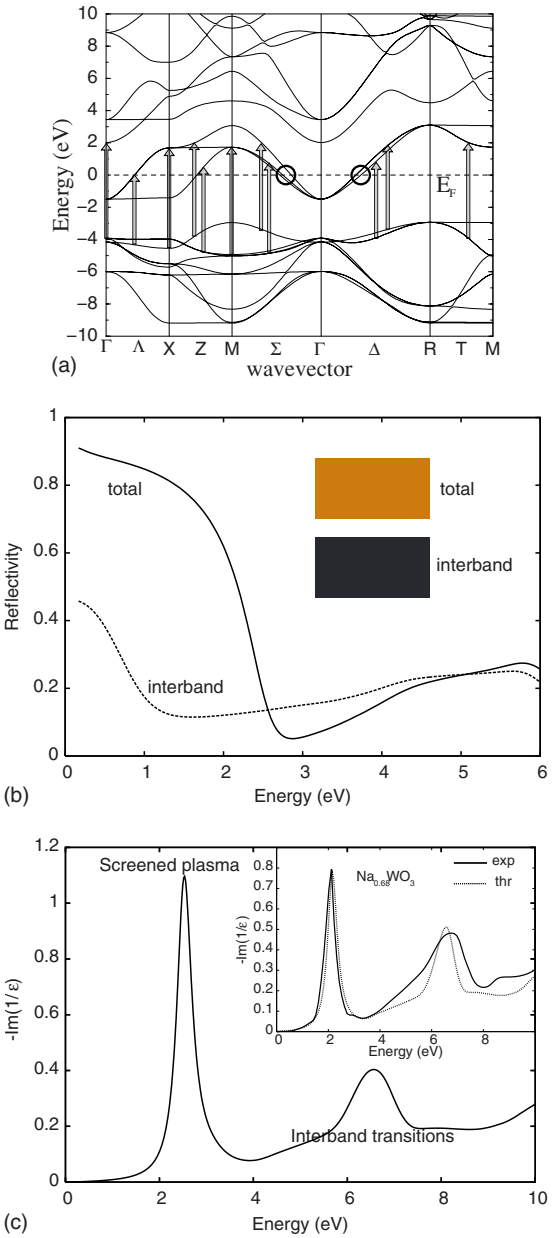

FIG. 2. (Color online) Band structure (top), reflectivity (middle), and loss function of $Na_{1.0}WO_3$ (bottom). Some strong interband transitions are indicated by shaded arrows. Strong intersubband transitions are indicated by circles. The reflectivity spectra are calculated with and without the free carriers' contributions. Inset in the middle figure shows the colors of $Na_{1.0}WO_3$ before and after taking into account the free carriers' response. Inset in the bottom figure compares our result to experiment (Ref. 19) for $Na_{0.68}WO_3$.

$\tilde{\omega}_p \approx [\omega_p^2/\epsilon_1^{\text{inter}}(0)]^{1/2}$, which can be measured in electron-energy-loss spectroscopy experiments. Figure 2(c) shows the calculated-loss spectra of $Na_{1.0}WO_3$. The inset of Fig. 2(c) compares the calculated-loss spectra of $Na_{0.68}WO_3$ to experiment.[19] Both the plasmon and interband excitations can be clearly identified and compared reasonably well to experiment.

Optical properties and the color of Na_xWO_3. The results for $Na_{1.0}WO_3$ encourages us to carry out a systematic study of the optical properties of Na_xWO_3, with the hope that a quantitative understanding of dramatic color change of Na_xWO_3 with varying x might be within the reach of today's first-principles electronic-structure techniques. Figure 3(c) shows the calculated reflectivity for $Na_xWO_3 (0.3 \leq x \leq 1.0)$. The onset of the free carriers' enhanced reflectivity shifts to shorter wavelengths as x increases. This is because the screened plasma frequency $\tilde{\omega}_p$ increases with increasing free-carrier concentration. These results agree very well with the measurements by Brown and Banks[26] and by Goldner *et al.*[36] except for an overall rescaling of the absolute magnitude of the reflectivity (likely due to sample quality and/or diffuse loss of light intensity).

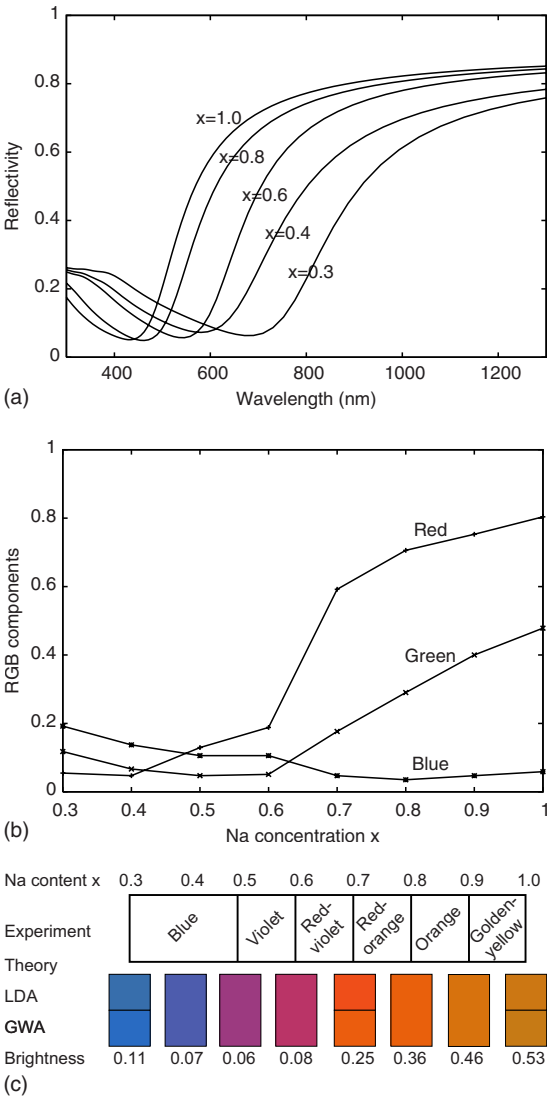

FIG. 3. (Color online) Calculated reflectivity spectra (top), the RGB tristimulus values (middle), and the color of Na_xWO_3 under uniform illumination (bottom).

With these results in hand, we are now ready to calculate the XYZ and RGB tristimulus values [defined in Eqs. (1) and (2)] of Na_xWO_3 and hence their colors. We assume that the illumination light source is uniform, i.e., $I(\lambda)$=constant in Eq. (1). Figure 3(b) shows the calculated RGB components as functions of x. Note that the RGB values are normalized to unity for perfect reflectors [$R(\lambda)=100\%$]. At low Na con-

centrations ($0.3 \leq x \leq 0.4$), the blue component dominates. This couples with the overall low reflectivity to give a dark bluish color for these systems as shown in Fig. 3(c). In order to better illustrate the *color*, the RGB tristimulus values are rescaled to give an even brightness in Fig. 3(c). The calculated values for the relative brightness are also shown in the figure. The brightness values are normalized such that a perfect reflector will have a brightness of unity.

As x increases beyond 0.6, both red and green components are greatly enhanced resulting in the red-orange to golden yellow metallic appearance of these systems [shown in Fig. 3(c)]. For intermediate Na concentration ($0.5 \leq x \leq 0.6$), red and blue components dominate; the systems thus appear violet to red-violet. Therefore, our theory is able to explain the systematic color change of Na_xWO_3 from dark blue to metallic golden yellow as x increases from 0.3 to 1.0. We mention that the description of color is somewhat subjective and it is not surprising that slightly different descriptions (e.g., purple vs violet)[1,8,9] of the apparent color of Na_xWO_3 are seen in literature.

To investigate the effects of electron-electron correlations on the optical properties, we have also carried out quasiparticle band-structure calculations within the GW approximation using the BERKELEYGW package. (One of the authors has been an active developer of the code over the years.) The results for Na_xWO_3 ($x=0.3$, 0.7, and 1.0) are reported at the bottom of Fig. 3. No appreciable changes in color are observed. This is expected since the optical properties of these systems in the visible window are dominated by the screened plasmon response and quasiparticle corrections do not affect the interband screening significantly. Electron-hole (i.e., excitonic) effects, although expected to be weak in these metallic systems, deserve further investigation.

In summary, we have carried out theoretical investigation of the optical properties and hence the color of Na_xWO_3. The apparent color is constructed using the CIE 1931 color-matching functions and the calculated reflectivity spectra. Our results clearly explain the systematic color change of Na_xWO_3 as x varies and provide direct evidence that the coloration of WO_3 upon charge insertion is a result of the subtle interplay between the interband and intraband optical responses. The reflectivity is greatly enhanced below the screened plasma frequency which explains the vivid color change of Na_xWO_3 as Na concentration increases. In addition, we demonstrate that first-principles electronic-structure theory can predict the apparent color of crystalline materials and may help to design materials with desired colors for various applications.

We thank M. D. Jones for his assistance in coding. This work was supported in part by the National Science Foundation under Grant No. CBET-0844720, and by the UB 2020 Interdisciplinary Research Development Fund (IRDF). We acknowledge the computational support provided by the Center for Computational Research at the University at Buffalo, SUNY.

[1] C. G. Granqvist, *Handbook of Inorganic Electrochromic Materials* (Elsevier, Amsterdam, 1995).
[2] C. G. Granqvist, G. A. Niklassan, and A. Azens, Appl. Phys. A **A89**, 29 (2007).
[3] S. K. Deb, Appl. Opt. **3**, 193 (1969).
[4] S. K. Deb, Philos. Mag. **27**, 801 (1973).
[5] H. Chen, N. Xu, S. Deng, J. Zhou, Z. Li, H. Ren, J. Chen, and J. She, J. Appl. Phys. **101**, 14303 (2007).
[6] C. Liao, F. Chen, and J. Kai, Sol. Energy Mater. Sol. Cells **90**, 1147 (2006).
[7] P. Hohenberg and W. Kohn, Phys. Rev. **136**, B864 (1964).
[8] J. B. Goodenough, in *Progress in Solid State Chemistry*, edited by H. Heiss (Pergamon, London, 1971), Vol. 5, pp. 144–399.
[9] S. Raj *et al.*, Phys. Rev. B **75**, 155116 (2007).
[10] B. W. Faughnan, R. S. Crandall, and P. M. Heyman, RCA Rev. **36**, 177 (1975).
[11] H. N. Hersh, W. E. Kramer, and J. H. McGee, Appl. Phys. Lett. **27**, 646 (1975).
[12] S. Hashimoto and H. Matsuoka, J. Appl. Phys. **69**, 933 (1991).
[13] P. M. S. Monk, Crit. Rev. Solid State Mater. Sci. **24**, 193 (1999).
[14] S. Z. Karazhanov, Y. Zhang, L. W. Wang, A. Mascarenhas, and S. Deb, Phys. Rev. B **68**, 233204 (2003).
[15] J. F. Owen, K. J. Teegarden, and H. R. Shanks, Phys. Rev. B **18**, 3827 (1978).
[16] M. A. Langell and S. L. Bernasek, Phys. Rev. B **23**, 1584 (1981).
[17] J. H. Davies and J. R. Franz, Phys. Rev. Lett. **57**, 475 (1986).
[18] R. G. Egdell and M. D. Hill, Chem. Phys. Lett. **85**, 140 (1982).
[19] M. Kielwein, K. Saiki, G. Roth, J. Fink, G. Paasch, and R. G. Egdell, Phys. Rev. B **51**, 10320 (1995).
[20] A. Hjelm, C. G. Granqvist, and J. M. Wills, Phys. Rev. B **54**, 2436 (1996).
[21] A. D. Walkingshaw, N. A. Spaldin, and E. Artacho, Phys. Rev. B **70**, 165110 (2004).
[22] B. Ingham, S. C. Hendy, S. V. Chong, and J. L. Tallon, Phys. Rev. B **72**, 075109 (2005).
[23] T. Smith and J. Guild, Trans. Opt. Soc., London **33**, 73 (1931).
[24] E. Salje and K. Viswanathan, Acta Crystallogr., Sect. A: Cryst. Phys., Diffr., Theor. Gen. Crystallogr. **31**, 356 (1975).
[25] A. S. Ribnick, B. Post, and E. Banks, *Advance in Chemistry Series* (American Chemical Society, Washington, DC, 1963), Vol. 39, p. 246.
[26] B. Brown and E. S. Banks, J. Am. Chem. Soc. **76**, 963 (1954).
[27] W. McNeill and L. E. Conroy, J. Chem. Phys. **36**, 87 (1962).
[28] W. Kohn and L. J. Sham, Phys. Rev. **140**, A1133 (1965).
[29] J. Ihm, A. Zunger, and M. L. Cohen, J. Phys. C **12**, 4409 (1979).
[30] http://www.nersc.gov/projects/paratec
[31] D. R. Hamann, M. Schlüter, and C. Chiang, Phys. Rev. Lett. **43**, 1494 (1979).
[32] N. Troullier and J. L. Martins, Phys. Rev. B **43**, 1993 (1991).
[33] H. J. Monkhorst and J. D. Pack, Phys. Rev. B **13**, 5188 (1976).
[34] L. Nordheim, Ann. Phys. **9**, 607 (1931).
[35] L. Bellaiche and D. Vanderbilt, Phys. Rev. B **61**, 7877 (2000).
[36] R. B. Goldner, G. Berrera, F. O. Arntz, T. E. Haas, B. Morel, and K. K. Wong, in *Electrochromic Materials*, edited by M. K. Carpenter and D. A. Corrigan (The Electrochemical Society, Pennington, 1990), Vol. 90–2, p. 14.